Journal of Non-Crystalline Solids 646 (2024) 123244

Contents lists available at ScienceDirect

Journal of Non-Crystalline Solids

journal homepage: www.elsevier.com/locate/jnoncrysol

Evolution of activation energy for boron dissolution in the borosilicate glass during the initial leaching stage

Kai Bai [a,b,c,1], Xiaofen Chen [d,1], Yuhe Pan [a,b,c], Zhaoxuan Jin [a,b,c], Buyun Zhang [a,b,c], Yuchuan Wang [a], Peng Lv [a,b,c], Tieshan Wang [a,b,c], Haibo Peng [a,b,c,*]

[a] School of Nuclear Science and Technology, Lanzhou University, Lanzhou 730000, China
[b] Key Laboratory of Special Function Materials and Structure Design Ministry of Education, Lanzhou University, Lanzhou 730000, China
[c] MOE Frontiers Science Center for Rare Isotopes, Lanzhou 730000, China
[d] College of Chemistry and Chemical Engineering, Lanzhou University, Lanzhou 730000, China

ARTICLE INFO

Keywords:
Borosilicate glass
Leaching behavior
ICP-OES
Apparent activation energy
FTIR

ABSTRACT

Borosilicate glass is widely used for immobilizing high-level radioactive waste. In this study, two types of borosilicate glasses, Na-borosilicate and Zr-Na-borosilicate, were subjected to leaching within a temperature range of 50–90 °C, at 10 °C intervals. The rate of boron consumption was measured by Inductively Coupled Plasma Optical Emission Spectrometer (ICP-OES) and Fourier-Transform infrared spectroscopy (FTIR) techniques, and the boron activation energy was determined through the Arrhenius equation. The boron activation energies for Na-borosilicate and Zr-Na-borosilicate glasses are approximately 46 kJ/mol and 42 kJ/mol, respectively. The activation energy, which FTIR calculated, was consistent with that obtained by ICP-OES during the initial leaching time and decreased as the leaching time increased. The decrease in activation energy of boron is because the [BO_3] structure was replaced by molecular water. The FTIR method offers an alternative approach for calculating the boron activation energy and contributes to understanding the leaching mechanism in the initial leaching stage.

1. Introduction

Nuclear power plants operation generates various levels of radioactive waste that require proper disposal. Vitrification and deep geological disposal are the widely adopted methods for managing high-level radioactive waste (HLW) [1–4]. Borosilicate glass is considered an ideal material due to its excellent thermal stability, high waste-loading capacity, and well-established preparation process [5,6]. Over the disposal period, typically spanning millions of years, the glass network structure may be compromised by radiation damage from radioactive nuclides and potentially corroded by groundwater. Numerous studies on water corrosion, encompassing glass-water reaction models and corrosion mechanisms, have been published over the past decades [7–20]. To investigate the corrosion behavior of HLW glass in water, leaching experiments under various conditions have been conducted [21–28].

The leaching behavior of HLW glass is influenced by numerous parameters such as glass composition [29–31] and radionuclide content [32], time [33], temperature [34], metal ion concentration in groundwater [35], and pH [36]. The relationship between activation energy and temperature follows the Arrhenius law. When the activation energy is influenced by two or more factors, it is referred to as the apparent activation energy. The apparent activation energy was determined by measuring the mass loss of various elements or the entire glass at different temperatures. The activation energy represents the energy barrier for the glass-water reaction [37]. Ojovan et al. [36] separated the activation energy into effective diffusion and hydrolysis energy components during the diffusion-controlled leaching stage. Vienna et al. [30] calculated the activation energies of 19 glasses based on the equation proposed by Helgeson et al. [38] and investigated the composition effect on glass forward dissolution rate. Jegou et al. [39] investigated the temperature effect on SON68 glass using the vapor hydration test (VHT), and calculated the activation energy based on the

* Corresponding author at: School of Nuclear Science and Technology, Lanzhou University, Lanzhou 730000, China.
E-mail address: penghb@lzu.edu.cn (H. Peng).
[1] These authors contributed equally to this work.

https://doi.org/10.1016/j.jnoncrysol.2024.123244
Received 21 June 2024; Received in revised form 14 September 2024; Accepted 24 September 2024
Available online 29 September 2024

equivalent thickness measured by Time-of-Flight Secondary Ion Mass Spectrometry (ToF-SIMS). Goût et al. [34] studied the temperature dependence of MW glass using the Product Consistency Test (PCT) method. Zapol et al. [40] calculated hydrolysis reaction barriers in a sodium borosilicate glass using density functional theory.

The studies mentioned above reported activation energies for various glasses. The activation energy of glass is constant under specific leaching conditions, representing the minimum energy required for a reaction to occur. For borosilicate glass, most of the boron atoms on the surface went into the water during the leaching process. Investigating the activation energy of boron can aid in optimizing the glass composition and developing products better suited for the vitrification of high-level radioactive waste. In this study, we propose a novel method for calculating the activation energy based on the boron structure in the infrared spectrum. This novel approach offers an alternative means of calculating the activation energy and yields reliable results.

2. Materials and methods

2.1. Sample preparation

In this study, two glass compositions were investigated: a ternary sodium borosilicate glass (NBS5) and a quaternary borosilicate glass (ZNBS1) prepared by incorporating zirconium into the ternary composition. The compositions and densities of these two glasses are listed in Table 1. The glasses were prepared following the same procedure as described in our previous studies [41,42]. The bulk glass was sectioned into standard specimens measuring 10 mm × 10 mm × 1 mm. Both surfaces of each specimen were polished.

2.2. Leaching experiment

Leaching experiments were conducted using the MCC-1 standard leaching method [43,44]. The leaching apparatus consisted of a stainless-steel autoclave and a 100 ml polytetrafluoroethylene (PTFE) container. A volume of 36 ml deionized water, saturated with CO_2 from the air, was used as the leaching solution. The ratio of the leachate volume to the glass surface area (V/SA) was maintained at 15 cm. Leaching experiments were performed at temperatures ranging from 50 °C to 90 °C, with increments of 10 °C. Before the experiments, the leaching vessels were preheated and equilibrated at the desired leaching temperatures. Samples were collected at various time points during the leaching process, with durations ranging from hours to days. After various time of leaching, the pH value of the leachate in both glasses does not exhibit a significant change.

2.3. Characterization methods

The concentration of boron, sodium, silicon, and zirconium in the leachate was determined by an Inductively Coupled Plasma Optical Emission Spectrometer (ICP-OES) which is from Analytik Jena AG company in Germany (instrument model: Plasma Quant PQ9000). The normalized mass loss (*NL*) of the element is defined by the following equation:

$$NL_i = \frac{C_i \times V}{f_i \times SA} \tag{1}$$

Table 1
The compositions and densities of the glasses.

Samples	Compositions/mol%				Density (g/cm^3)
	SiO_2	B_2O_3	Na_2O	ZrO_2	
NBS5	67.26	18.60	14.14	–	2.44
ZNBS1	60.20	19.80	18.30	1.70	2.51

where NL_i is the normalized mass loss of the i^{th} element, g/m^2; C_i is the concentration of i^{th} element that was measured by ICP-OES, g/ml; V is the volume of leachate, ml; f_i is the mass fraction of i^{th} element in pristine glass; SA is the surface area of samples, m^2. Considering temperature fluctuations and time errors during the experiment, the relative uncertainty of NL_i was estimated to be less than 10% [45].

Fourier-transform infrared (FTIR) spectroscopy was employed to characterize the structural features of the borosilicate glasses. The FTIR spectra were acquired using a Spectrum Two spectrometer (PerkinElmer, Inc., USA) equipped with an attenuated total reflectance (ATR) accessory. All measurements were performed at room temperature over a spectral range of 500 cm^{-1} to 4000 cm^{-1} with a resolution of 2 cm^{-1}. To ensure the reproducibility and representativeness of the data, each spectrum was collected by averaging 10 scans, and four spectra were obtained from different regions of each glass sample.

The Time-of-Flight Secondary Ion Mass Spectrometry (ToF-SIMS, IONTOF GmbH) was employed to investigate the depth profile of NBS5 glasses after leaching at a certain time. The vacuum in the target chamber was at a level of 10^{-7} Pa during the measurement. The Cs^+ ions, with an energy of 2 keV, were used for sputtering the surface. The analysis utilized a 25 keV monatomic Bi^+ beam (~1.0 pA) operating at a 10 kHz frequency. Negative ions were selected for analysis, and a flood gun was used throughout to counteract any charging effect. Depths were gauged using a profilometer, correlating linearly with sputtering time. The sputtering area was set to 150 × 150 μm^2, and the analysis area was 40 × 40 μm^2.

2.4. Calculating methods for activation energy

The activation energy of elemental release from the glass matrix can be determined using the Arrhenius equation [36,46,47], which describes the temperature dependence of the reaction rate constant. The Arrhenius equation is expressed as follows:

$$k(i) = A \times exp\left(\frac{-E_a(i)}{RT}\right) \tag{2}$$

where $k(i)$ is the reaction rate obtained by dividing the concentration of i^{th} element (measured by ICP-OES) into the leaching time, g/(L·d); $E_a(i)$ is the activation energy of i^{th} element, kJ/mol; R is the ideal gas constant and the value is 8.314 J/(mol·K); T is the absolute temperature, K; A is Arrhenius parameter.

By plotting the natural logarithm of the reaction rate constant ($ln\ k$) against the reciprocal of the absolute temperature ($1/T$), the activation energy can be determined from the slope of the linear regression line, which is equal to $-E_a/R$. This approach allows for the quantification of the energy barrier that must be overcome for the release of elements from the glass structure during the leaching process.

In addition to the conventional method of calculating the reaction rate constant (k) from the concentration of released elements in the leachate, an alternative approach can be employed by analyzing the change in the peak area of boron-related structures in the FTIR spectrum. This method is based on the decrease in the peak area of boron-related vibrations is equivalent to the extent of boron release from the glass structure during leaching. The reaction rate constant can be calculated using the following equation:

$$k = \Delta[BO_3] = I_P - I_D \tag{3}$$

where $\Delta\ [BO3]$ is the intensity variation of [BO_3] structure which is located from 1250 cm^{-1} to 1550 cm^{-1} through infrared spectra, I_P is the integral area of [BO_3] structure in the infrared spectrum of pristine glass, and I_D is the integral area of [BO_3] structure after different leaching time. Fig. 1 presents the FTIR spectrum of NBS5 pristine glass and the spectra obtained after various leaching durations at 90 °C. The peak intensity of the [BO_3] structure, located between 1250 cm^{-1} and 1550

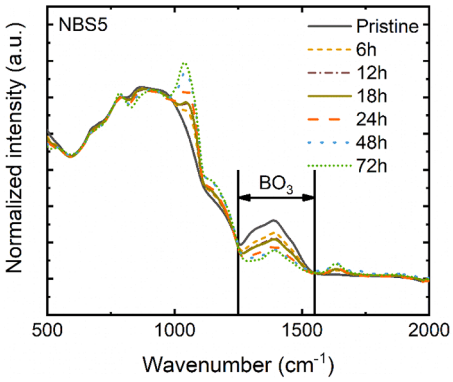

Fig. 1. The infrared spectra of NBS5 glass after different leaching times at 90 °C.

cm^{-1}, decreases with increasing leaching time. By employing this method, boron's reaction rate constant (k) can be determined at different leaching times using the FTIR spectra, and the activation energy for boron can be calculated using Eq. (2). This approach for determining the activation energy is referred to as the FTIR method, while the conventional approach based on leachate analysis is called the ICP-OES method.

3. Results

3.1. Solution analysis

Fig. 2 presents the normalized mass loss (*NL*) of the main elements in NBS5 and ZNBS1 glasses as a function of leaching time at 70 °C. The *NL* of the main elements at other temperatures are provided in Supplementary Figs. A.1–8. As shown in Fig. 2, during the first 18 h, the *NL* of boron, silicon, and sodium from NBS5 glass increases linearly with the square root of leaching time, indicating that the leaching process is controlled by interdiffusion [36]. After 18 h of leaching, the normalized mass loss of boron ceased to show a linear correlation with the square root of time, which indicates that the mechanism of boron leaching has changed, with the increase of silicon release also implying that an increasing contribution from network hydrolysis to the boron mass loss. In ZNBS1 glass, the *NL* of boron, silicon, and sodium increases linearly with the square root of leaching time throughout the entire leaching period. The dominant mechanism at the water-glass reaction interface is interdiffusion within the time range covered by the fitting line. The *NL* of zirconium is not presented because its concentration in the leachate was below the detection limit. The *NL* of silicon in ZNBS1 glass is significantly lower than in NBS5 glass, indicating that ZNBS1 glass exhibits better leaching resistance than NBS5 glass.

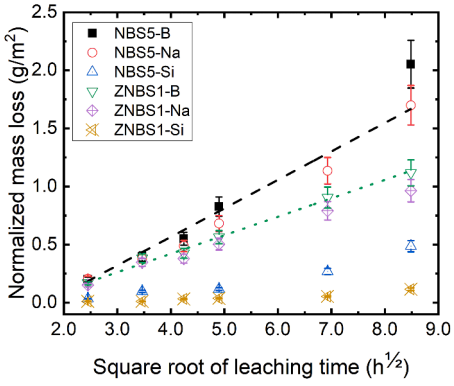

Fig. 2. Normalized mass loss (*NL*) of B, Na, and Si in NBS5 and ZNBS1 glasses obtained through ICP-OES over square root of leaching time at 70 °C.

The initial leaching rate (r_0) is another parameter used to assess the leaching resistance of glass. In this study, linear regression of the silicon *NL* data determined the initial leaching rate within the first 24 h of leaching. The details of the fitting process are presented in Supplementary Fig. A.9. The initial leaching rates of NBS5 and ZNBS1 glasses at 70 °C were found to be 0.11±0.02 g/(m^2•d) and 0.02±0.01 g/(m^2•d), respectively. The initial leaching rate of NBS5 glass is approximately five times higher than that of ZNBS1 glass at 70 °C.

3.2. Microstructure evolution

Fig. 3 presents the FTIR spectra of NBS5 and ZNBS1 glasses subjected to different leaching times at 70 °C. All spectra were normalized with a wavenumber of 585 cm^{-1}. The FTIR spectra of both glasses at other temperatures are provided in Supplementary Figs. A.10–17. As shown in Fig. 3, the decrease or increase in peak intensity indicates significant changes in the corresponding microstructures. For both NBS5 and ZNBS1 glasses, the peak intensity between 1250 cm^{-1} and 1550 cm^{-1}, which is attributed to [BO_3], decreases with leaching time [48,49]. The peak located at 1050 cm^{-1}, which corresponds to the stretching vibration of the Si-O-Si bond in the Q^3 structural unit (where Q represents the SiO_4 tetrahedron and n is the number of bridging oxygens) [50], increases in intensity with leaching time. The increase in the peak intensity at 1633 cm^{-1} with leaching time suggests enhanced diffusion of molecular water into the glass network structure [51,52]. The peak intensity between 2700 cm^{-1} and 3700 cm^{-1}, which is assigned to the vibrations of molecular water and hydroxyl groups, significantly increases with leaching time [22,48].

In addition to the four peaks displaying significant changes, another peak around 840 cm^{-1}, which is attributed to the [BO_4] structure units, decreases in intensity with leaching time [53]. ZNBS1 glass exhibits the same trends in the aforementioned characteristic signals as NBS5 glass, except for the Q^3 and hydroxyl structural units. It is worth noting that, for the same leaching time, the peak intensity of the Q^3 structural unit is more pronounced in NBS5 glass compared to ZNBS1 glass. In contrast, the peak comprising hydroxyl groups and molecular water in ZNBS1 glass exhibits a more pronounced change than that in NBS5 glass, suggesting a higher concentration of water molecules in ZNBS1 glass for the same leaching time.

Fig. 4 illustrates the evolution of the [BO_3] peak intensity with the leaching time. With increasing leaching time, the intensity of the [BO_3] peak decreases and eventually reaches a plateau. Although the intensity of the [BO_3] peak has not dropped to zero, the area of the [BO_3] peak does not change significantly over time. Therefore, the values of 500 and 360 from original statistics are chosen as the exhaustion limits for [BO_3] in NBS5 and ZNBS1glass, respectively. Supplementary Fig. A.18 illustrates the relationship between the effective infrared detection depth and the wavenumber. Fig. 5 presents the evolution of other characteristic peaks for NBS5 and ZNBS1 glasses. For both NBS5 and ZNBS1 glasses, the intensities of the molecular water peak increased linearly and did not reach a saturation limit at lower temperatures. Saturation of the peak intensity was observed after 1 day of leaching at higher temperatures of 80 °C and 90 °C. It is noteworthy that the evolution of the hydroxyl peak differs between NBS5 and ZNBS1 glasses. In NBS5 glass, the hydroxyl peak intensity increased linearly and approached saturation after 3 days of leaching. In contrast, the hydroxyl peak intensity in ZNBS1 glass exhibited a more pronounced change and reached saturation after 2 days of leaching at a higher temperature of 80 °C.

Fig. 6(a) presents the exhaustion time of the [BO_3] structural units and the saturation time of molecular water for NBS5 and ZNBS1 glasses. Both time scales decrease with increasing temperatures. Notably, the exhaustion of [BO_3] structural units occurs within approximately 30 h at 90 °C for both glasses. When the temperature is at 50 °C, the exhaustion times increase by factors of 6 and 9 for NBS5 and ZNBS1 glass, respectively. Fig. 6(b) illustrates the ratio of the [BO_3] structural unit exhaustion time to the molecular water saturation time. For NBS5 glass,

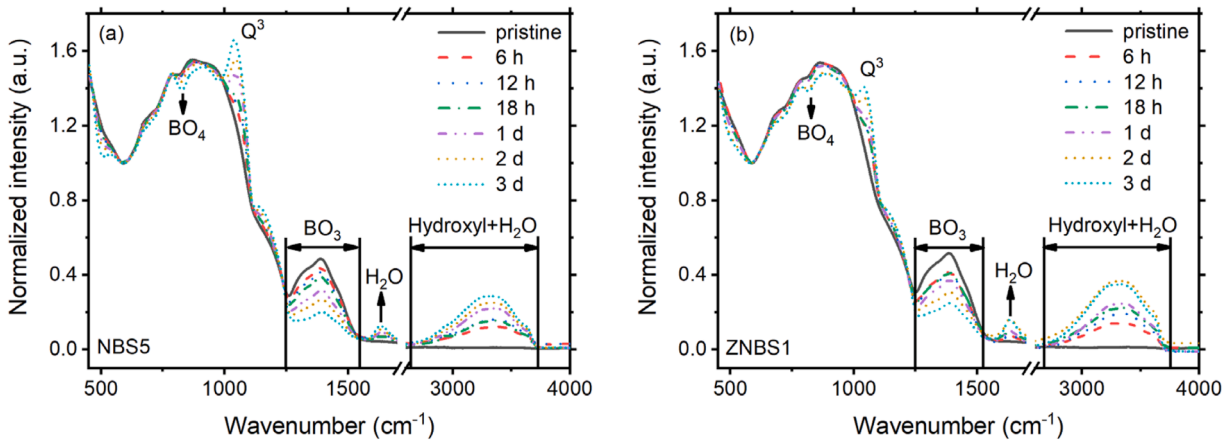

Fig. 3. The infrared spectra of NBS5 (a) and ZNBS1 (b) glasses with different leaching times at 70 °C.

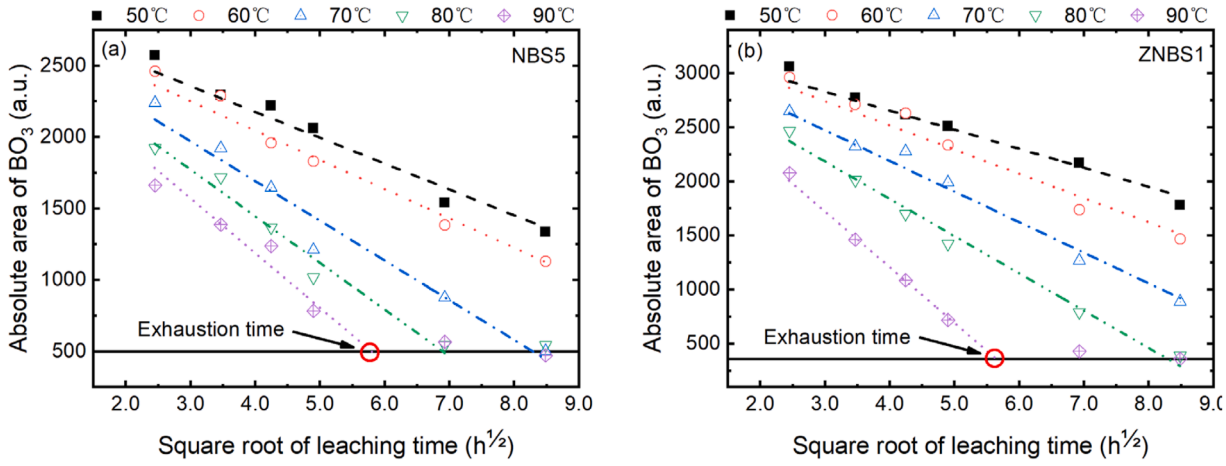

Fig. 4. The change of [BO_3] with leaching time for NBS5 (a) and ZNBS1 (b) glasses. (The saturation limit is 500 and 360 for [BO_3] in NBS5 and ZNBS1 glass, respectively. The values 500 and 360 are the results of the original statistics.).

the ratio increases linearly with temperature, while for ZNBS1 glass, the ratio remains nearly constant with varying temperatures. The nearly constant ratio suggests that the rate of boron leaching and water penetration are nearly identical in ZNBS1 glass. The difference in the ratios may be attributed to the distinct compositions of the two glasses.

3.3. Activation energy

Fig. 7 presents the activation energies determined by the ICP-OES method for boron, E_a(B), and sodium, E_a(Na), in NBS5 glass at various leaching times. As shown in Fig. 7(a), the red dash line, blue dot line, dark yellow short dot line, and brown dash-dot line correspond to leaching times of 6 h, 8 h, 1 day, and 3 days, respectively, parallel each other. This suggests that E_a(B) remains constant within the margin of error, with a value of approximately 46 kJ/mol. Likewise, Fig. 7(b) illustrates the linear fits for E_a(Na) at different leaching times. The value of E_a(Na) is approximately 36 kJ/mol.

The E_a(B), determined from the FTIR spectrum, was calculated based on the change in the [BO_3] structural units. A similar approach was employed to calculate E_a(B), with the rate constant (k) determined from the FTIR spectra. The linear fitting results are presented in Fig. 8, and the activation energies are summarized in Table 2. At the initial time of leaching, the linear fits are parallel, indicating that the E_a(B) values are nearly identical. As the leaching time increases, the slope of the fitting line decreases, resulting in a reduction in the activation energy. After 18 h of leaching, the activation energy obtained using the FTIR method might be inaccurate due to the thickness of the altered layer beyond the effective penetration depth of FTIR. At the same leaching time, the normalized mass loss of boron deviated from the linear relationship with the square root of leaching time. In NBS5 glass, the E_a(B) determined by the FTIR method decreases with leaching time and reaches a stable value after two-day leaching.

The same activation energy calculation approach including ICP-OES and FTIR methods was employed for ZNBS1 glass. Fig. 9 presents the ICP-OES method calculated activation energies of boron, E_a(B), and sodium, E_a(Na), in ZNBS1 glass. The values of E_a(B) and E_a(Na) are approximately 42 kJ/mol and 37 kJ/mol, respectively. In ZNBS1 glass, the activation energy E_a(B) is lower than that of NBS5 glass and E_a(Na) is very similar to that in NBS5 glass. This difference may be attributed to the distinct compositions of the two glasses.

The E_a(B) in ZNBS1 glass calculated using the FTIR method at various leaching times is exhibited in Supplementary Fig. A.19. As with NBS5 glass, the activation energy of boron in ZNBS1 glass decreases with increasing leaching time. Table 2 summarizes the values at different leaching times and Fig. 10 illustrates the evolution of E_a(B) in NBS5 and ZNBS1 glasses as a function of leaching time, calculated using both ICP-OES and FTIR methods. The activation energies obtained by the FTIR method after various leaching times in both glasses exhibited a decreasing trend. The decreasing trend of E_a(B) determined by the FTIR method was fitted with a linear function, yielding a high R^2 value better than 0.95. The red solid line represents the E_a(B) of NBS5 glass calculated using the ICP-OES method, while the black dashed line

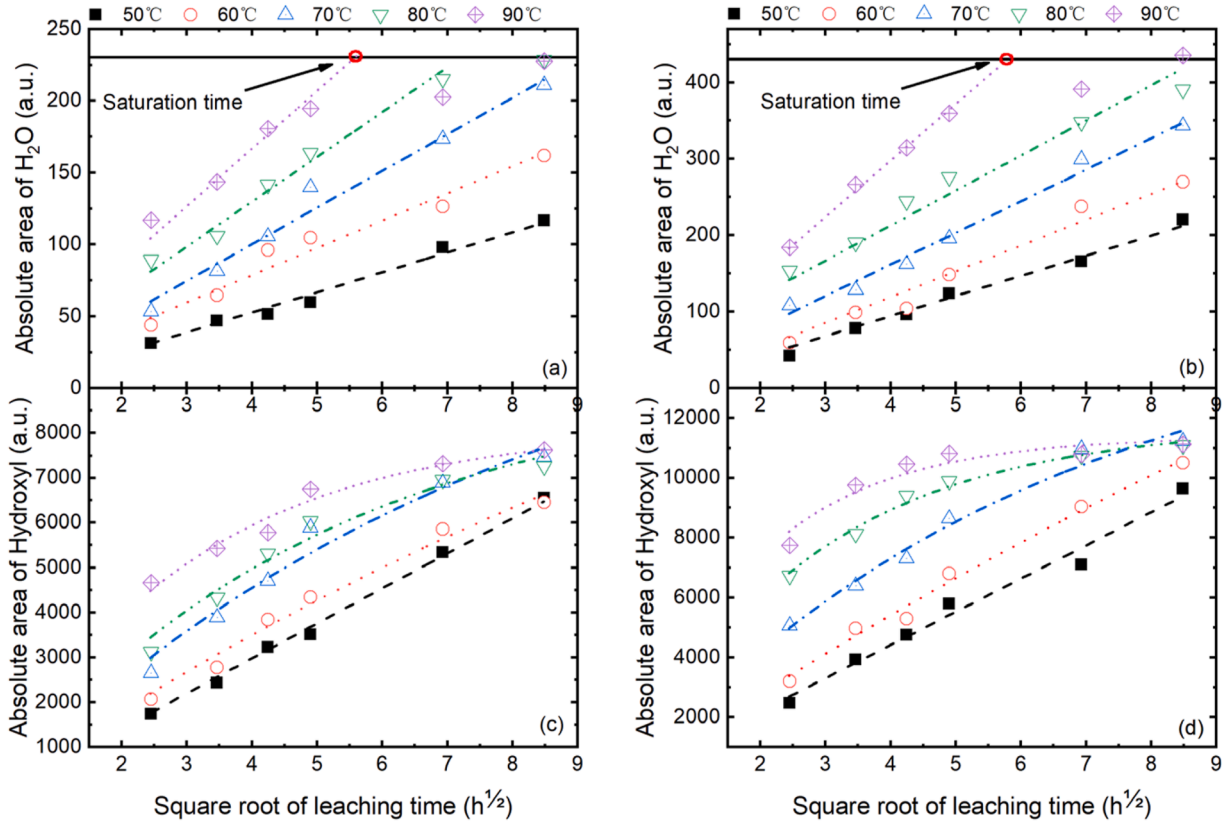

Fig. 5. The evolution of characteristic peaks for NBS5 and ZNBS1 glasses with leaching time. ((a) The molecular water of NBS5 glass; (b) The molecular water of ZNBS1 glass; (c) The hydroxyl of NBS5 glass; (d) The hydroxyl of ZNBS1 glass.).

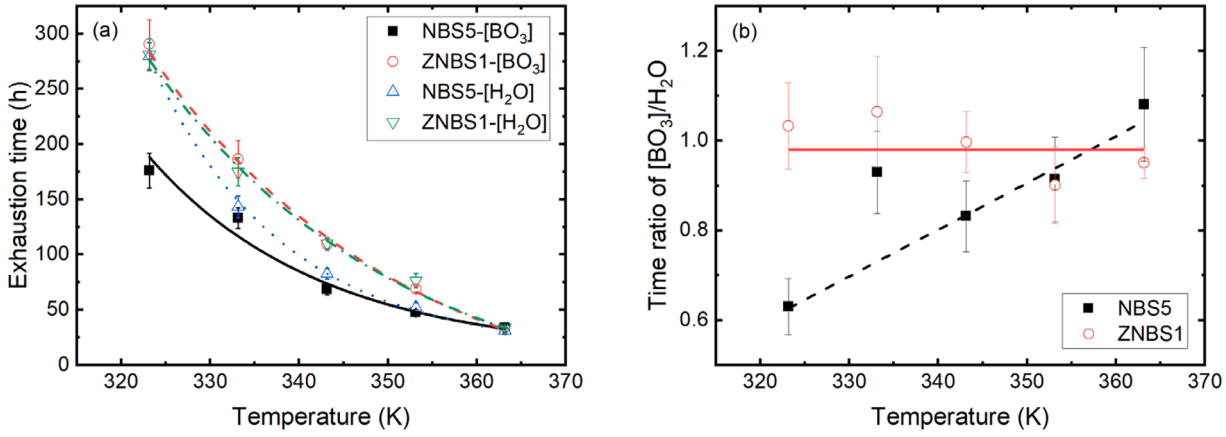

Fig. 6. The relationship between the exhaustion time, saturation time, and leaching temperature, as well as their interdependence. (a) Exhaustion time and saturation time as a function of leaching temperature for NBS5 and ZNBS1 glasses; (b) Ratio of the [BO_3] structural unit exhaustion time to the molecular water saturation time.

corresponds to the FTIR method. The E_a(B) values for NBS5 glass calculated using these two methods intersect at a leaching time of more than 4 h. For ZNBS1 glass, the green dotted line represents the E_a(B) obtained using the ICP-OES method, while the blue dash-dotted line corresponds to the linear fit of the FTIR data. The intersection occurs at a leaching time of less than 4 h. These results confirm that the method for calculating E_a(B) using FTIR spectra applies to both ternary and quaternary borosilicate glasses with a significant change of boron-related structure in the infrared spectrum.

As the [BO_3] structural units disappear from the glass network, the corresponding volume is replaced by molecular water, exhibiting a strong linear relationship between the two [41]. Fig. 11 illustrates the relationship between the integrated area of molecular water and the E_a(B). The increase in molecular water content is linearly related to the decrease in E_a(B), suggesting that interdiffusion plays an important role in the leaching mechanisms of boron. In contrast, the decrease in E_a(B) positively correlates with the change in the proportion of [BO_3] structural units. A higher proportion of [BO_3] structural units allows for the accommodation of more molecular water, resulting in a stronger linear trend observed in ZNBS1 glass.

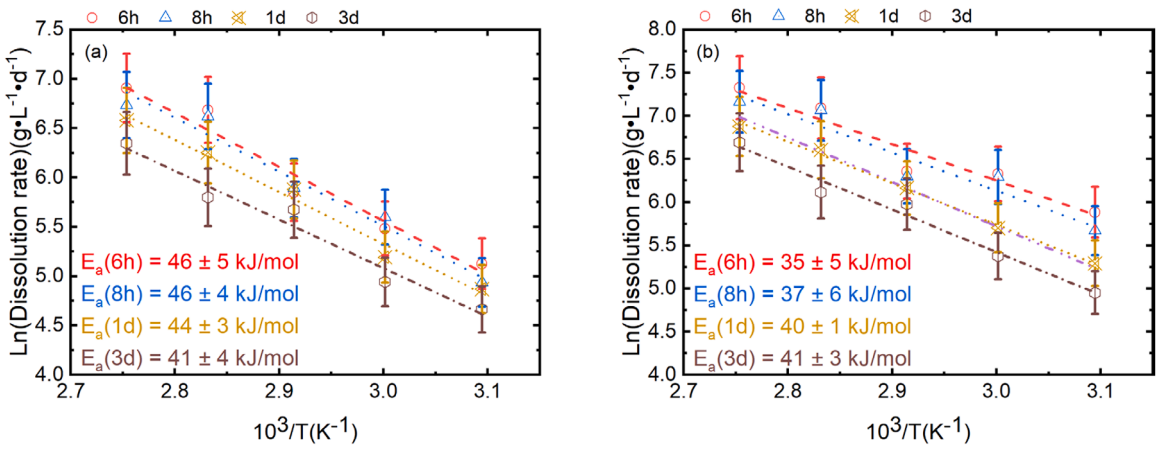

Fig. 7. Activation energies of boron (a) and sodium (b) calculated by ICP-OES method in NBS5 glass at various leaching time.

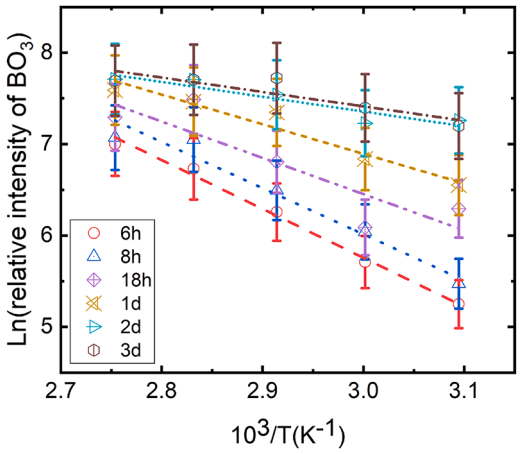

Fig. 8. E_a(B) in NBS5 glass calculated by the FTIR method after various leaching durations.

Table 2
The E_a(B) in NBS5 and ZNBS1 glass as a function of time measured by FTIR method.

Time (h)	6	8	12	18	24	48	72
NBS5-E_a(B) (kJ/mol)	45 ±2	42 ±5	35 ±5	33 ±10	27 ±4	14 ±3	13 ±4
ZNBS1-E_a(B) (kJ/mol)	39 ±6	39 ±3	38 ±4	36±3	30 ±2	25 ±2	20 ±3

4. Discussion

4.1. The role of zirconium

The normalized mass loss of the main elements and the initial leaching rate (r_0) of silicon in ZNBS1 glass are lower than those of NBS5 glass. The intensity of the characteristic peaks at 1050 cm^{-1} in ZNBS1 glass is lower than that of NBS5 glass. ICP-OES and FTIR results suggest that incorporating zirconium into the glass network structure will reduce silicon release. As the main component of the glass network structure, the reduction in silicon release means that the depolymerization of the glass network is weakened, further illustrating that the ZNBS1 glass has better leaching resistance [54,55]. Several studies have reported that incorporating zirconium can improve the macroscopic properties of glass, such as hardness [56]. On a microscopic level, incorporating zirconium can strengthen the bonds within the glass network. This is particularly true for the many 6-coordinated zirconium conformations, which makes the glass more resistant to leaching [55, 57].

The apparent activation energy of boron, E_a(B), shows the opposite results. The E_a(B) of ZNBS1 glass is very close to that of NBS5 glass, and it is even lower 4 kJ/mol than that of NBS5 glass. E_a(B) can be considered the minimum energy required for boron in the glass network to react with water. The lower activation energy suggests that the boron in ZNBS1 glass reacts more easily with water than that in NBS5 glass. Fig. 12 shows the element distribution of NBS5 glass measured by TOF-SIMS after different leaching times at 90 °C. The intensities of other elements were normalized relative to the intensity of silicon. As the leaching time increases, the interface depth of boron and sodium continues to deepen, and the changes in depth for both elements are nearly identical. Gin et al. [8] reported that the thickness of the altered layer in glass could be determined by dividing the normalized mass loss of boron into the glass density. Table 3 shows the interface depth of boron in NBS5 and ZNBS1 glass calculated by ToF-SIMS and ICP-OES at the same leaching time and leaching temperature at 90 °C. The results show that zirconium doping does not reduce the release rate of boron from the glass network. It is noted that the boron interface depth calculated by ICP-OES is deeper than that of ToF-SIMS. The reason might be the leaching mechanism is controlled by both interdiffusion and network hydrolysis. The ToF-SIMS boron interface depth is only the depth for interdiffusion, when the measurement has proceeded, a certain thickness of the altered layer has been peeled into the leachate. However, the detachment phenomenon would not affect the boron interface depth calculated by ICP-OES, which leads to the ToF-SIMS boron interface depth lower than that of ICP-OES. The discrepancy between these two methods might be the thickness of the altered layer peeled into the leachate.

On the other hand, the boron interface is deeper than ternary glass with the same leaching time in zirconium-doped glass indicating that the boron dissolution rate in ZNBS1 glass is more rapid. Cailleteau et al. [13] used the dissolved fraction of boron to quantify the effect of different zirconium contents on the altered layer in the ISG glass (without Al_2O_3). The results showed that replacing silica with zirconium can reduce the glass's dissolution kinetics but strengthen the boron's dissolved fraction. In this study, zirconium doping increases the leaching resistance of ZNBS1 glass, resulting in a lower silicon initial leaching rate of ZNBS1 compared to NBS5. Similarly, it will also increase the dissolved fraction of boron in ZNBS1 glass, which could also explain why the boron interface is deeper with the same leaching time in zirconium-doped glass and keeping the interdiffusion process during the three-day leaching time.

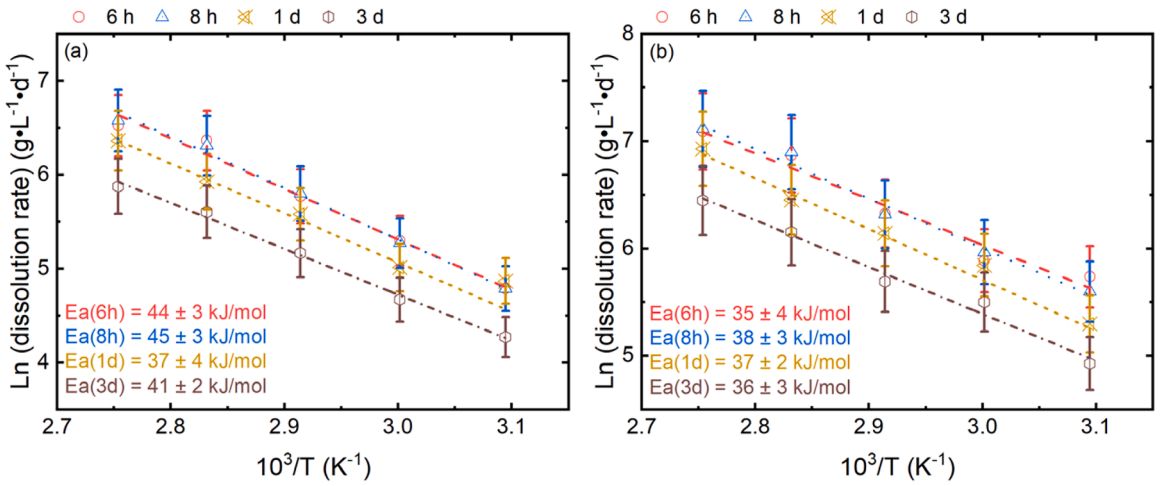

Fig. 9. Activation energies of boron (a) and sodium (b) calculated by the ICP-OES method in ZNBS1 glass at various leaching times.

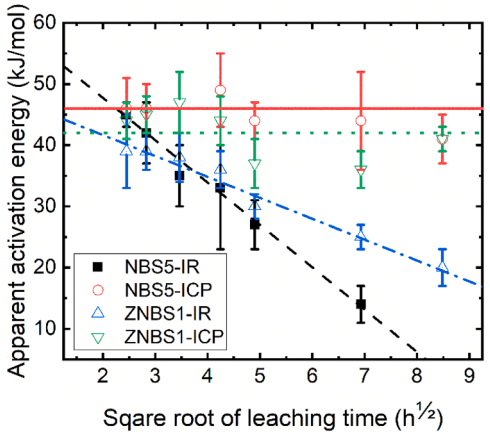

Fig. 10. The E_a(B) variation in NBS5 and ZNBS1 glass with leaching time. (The red solid line and green dotted line represent the E_a(B) of NBS5 and ZNBS1 glass calculated by the ICP-OES method, respectively. The black dashed line and blue dash-dotted line are the linear fittings of E_a(B) in NBS5 and ZNBS1 glass determined by the FTIR method, respectively.).

4.2. Temperature effect

When the glass is fully immersed in water, the interaction mechanism between borosilicate glass and water primarily involves the following processes: (I) Interdiffusion, including the ion exchange, occurs between the sodium ions from the glass modifier and the H^+/H_3O^+ in the aqueous solution, and the solid-liquid interdiffusion between glass and water [58]; (II) network hydrolysis, wherein the hydrolysis of the glass network leads to the release of network-forming elements such as silicon, boron, and network modifier sodium into the solution; (III) condensation, a surface alteration layer forms at the reaction interface between glass and water, which reduces both the glass dissolution rate and the release rate of network elements; (IV) secondary phases precipitation, depending on the glass composition and alteration conditions [10,59,60]. During the initial leaching period (within 3 days), (I) and (II) are the main interaction mechanisms in the glass-water leaching reaction.

Table 4 presents the initial leaching rates of silicon in NBS5 and ZNBS1 glass across various leaching temperatures. The fitting method has been previously described. At lower temperatures (50, 60, and 70 °C), the initial leaching rate exhibits only minor variations. Conversely, at higher temperatures (80 and 90 °C), the initial leaching rate changes significantly. Owing to zirconium doping, the release of silicon in ZNBS1 glass is not significant. However, the release of silicon in NBS5 glass at high temperatures is more pronounced, increasing markedly at 80 °C, and showing multiple times increase at 90 °C. With rising temperatures,

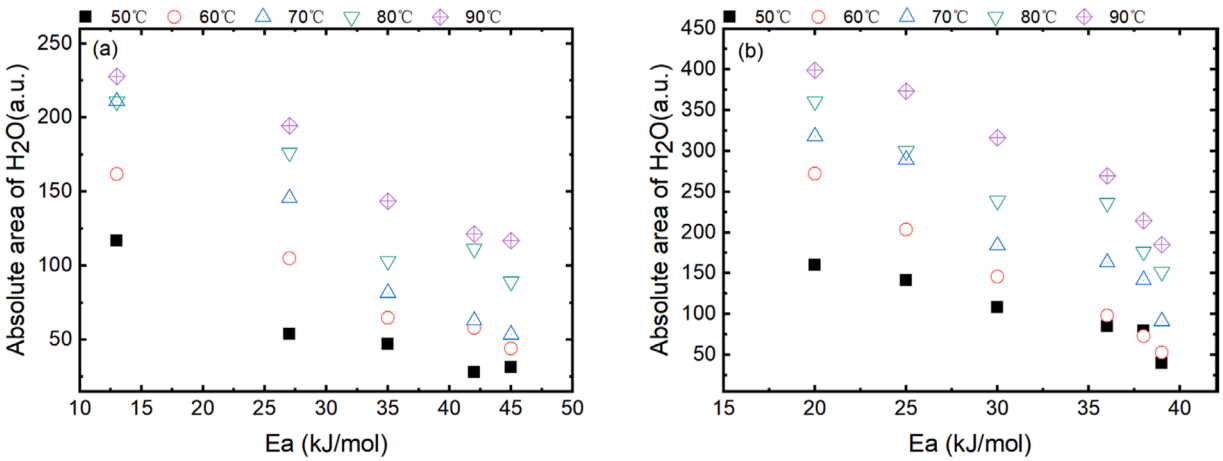

Fig. 11. The change of molecular water in NBS5 (a) and ZNBS1 (b) glasses with activation energy of boron.

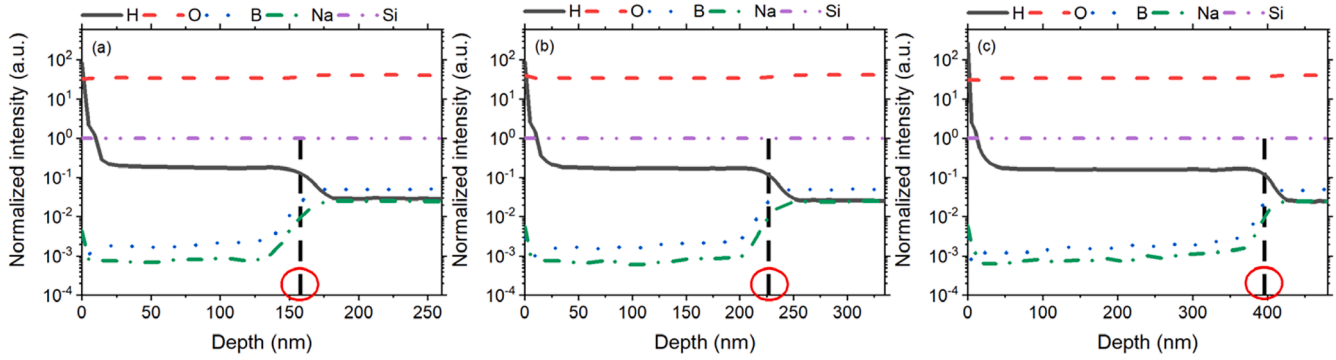

Fig. 12. Element distributions over the depth for NBS5 glass after different leaching times at 90 °C. (The black dash lines refer to the half maximum value of Boron intensity. (a), (b), and (c) are the leaching profiles for NBS5 glass after 6 h, 12 h, and 24 h leaching, respectively.).

Table 3
The boron interface depth measured by ToF-SIMS and ICP-OES after different leaching times at 90 °C.

Sample/leaching time (h)	Boron interface depth (nm)			
	NBS5		ZNBS1	
	ToF-SIMS	ICP-OES	ToF-SIMS*	ICP-OES
6 h	158	238	189	144
12 h	227	352	237	255
18 h	322	608	–	386
24 h	395	684	410	492

* The relevant data from Ref. [41].

Table 4
The initial leaching rate of silicon in NBS5 and ZNBS1 glass over various leaching temperatures.

Sample/ Temperature (°C)	Initial leaching rate (r_0) / ($g•m^{-2}•d^{-1}$)				
	50	60	70	80	90
NBS5	0.041 ±0.015	0.084 ±0.013	0.106 ±0.027	0.683 ±0.060	1.648 ±0.074
ZNBS1	0.003 ±0.001	0.013 ±0.006	0.018 ±0.009	0.120 ±0.013	0.566 ±0.069

the initial leaching rates exhibit an exponential increase, particularly notable change at elevated temperatures. Temperature has a significant effect on the initial leaching rate of silicon, especially for the simple ternary borosilicate glass.

The supplementary Figs. A.1–8 present the linear regression values of the normalized mass loss of boron versus the square root of time after leaching at various temperatures. For NBS5 glass, the normalized mass loss of boron within 18 h is proportional to the square root of time at all temperatures, indicating that the primary mechanism of boron leaching during this period is interdiffusion. At longer leaching times, the dominant mechanism might change, the boron interface depth calculated by ICP-OES is deeper than that measured by ToF-SIMS (as shown in Table 3) implying that the contribution of network hydrolysis would be strengthened. For ZNBS1 glass, the normalized mass loss of boron within 18 h is proportional to the square root of time at 50 °C and 60 °C. At higher temperatures (70 °C, 80 °C, and 90 °C), the normalized mass loss of boron over 3 days is proportional to the square root of time. This suggests that the leaching of boron in ZNBS1 glass within the initial 18-hour leaching time at all temperatures is governed by interdiffusion, while the leaching mechanism at high temperatures remains constant after 18 h of leaching might be caused by the altered layer hindering the release of boron from the glass network. The boron interface depths calculated by ICP-OES and ToF-SIMS (as presented in Table 3) are nearly identical also proving this statement.

4.3. The difference in activation energy calculated by two methods

The activation energy, E_a, calculated by ICP-OES is constant, reflecting that the element has already been released into the leachate when the measurement is performed. The activation energies of boron in the NBS5 and ZNBS1 glass, calculated using the ICP-OES method, were 46 and 42 kJ/mol, respectively. These values are lower than the activation energy of SON68 glass (62±13 kJ/mol) [39], a low-level radioactive waste solidification glass (52–56 kJ/mol) [61], and close to the activation energy of British MW glass (44.6 ± 2.9 kJ/mol) [34]. The activation energies for network hydrolysis (a surface-controlled reaction) and ion exchange (diffusion transport) are approximately 60 and 10 kJ/mol, respectively, while the activation energy for the combined mechanisms ranges from 15 to 50 kJ/mol [61]. The activation energy of boron falls within this range of mixed reactions, implying that the boron leaching mechanism mentioned above might involve both interdiffusion and network hydrolysis. However, the linear relationship between the normalized mass loss of boron and the square root of time does not corroborate this conclusion, particularly for ZNBS1 glass.

The activation energy of boron, E_a(B), calculated using the FTIR method, decreased with leaching time. As the leaching reaction proceeds, the [BO_3] structure within the glass network gradually disappears, with the remaining space being occupied by molecular water. This increase in molecular water diminishes the [BO_3] intensity as observed in the infrared spectrum, consequently lowering the activation energy calculated via the FTIR method. Fig. 11 illustrates the relationship between the activation energy decrease and the molecular water content increase. In the leaching process, an alteration layer gradually forms on the glass surface, and the formation time of this layer decreases with increasing temperature [34]. The alteration layer is a porous and loose structure [10,28,34,62], which might facilitate the subsequent leaching behavior as a diffusion transport process. However, the activation energy obtained by the ICP-OES method does not reflect this phenomenon. The possible reason is that the alteration layer might decrease the concentrations measured by ICP-OES and peel into the leachate. On the other hand, the decrease in activation energy for boron dissolution might imply that it gets easier with time to remove boron from the glass network by hydrolysis or interdiffusion. The reasonable assumption for reduced E_a(B) is, that after leaching, the [BO_3] structures might remain on the glass surface and form a high-concentration solution of boron, the difference in concentration would help the leaching process of boron. More important is that the structure of [BO_3] would be replaced by molecular water and the molecular water also might help in the leaching reaction. The aforementioned hypothesis might facilitate the leaching process, resulting in a decrease in the activation energy calculated using the FTIR method over leaching time.

Boron-related structures in glass comprise [BO_3] and [BO_4] structural units, the FTIR spectroscopy can reveal these structures. However, due to the influence of high background, the FTIR method can only

demonstrate changes in the [BO_3] structural units. Changes in the [BO_4] structural units are relatively minor, resulting in nearly identical dissolution rates (k) calculated based on the changes in [BO_4] structural units. During the leaching process, [BO_4] is first converted into [BO_3] [63], which affects the intensity of the [BO_3] structure. However, as the reaction continues, similar transformations occur at different depths. Fig. 12 indicates that the interface depths of boron and sodium are essentially the same. This suggests that [BO_4] within the leaching depth has been transformed into [BO_3], making it feasible to calculate the apparent activation energy based on [BO_3].

5. Conclusion

In this study, ternary and quaternary borosilicate glasses were subjected to leaching at various temperatures. After leaching, the glasses were analyzed with ToF-SIMS, FTIR, and concentrations of B, Na, Si, and Zr in the leached solution were measured with ICP-OES. The initial leaching rates of ternary and quaternary borosilicate glasses were obtained. Although Zr-Na-borosilicate glass exhibits better leaching resistance, zirconium doping increases the dissolved fraction of boron and provides more free volume to accommodate molecular water. The activation energy of boron calculated by the ICP-OES method remains constant. FTIR spectroscopy revealed changes in boron-related structural units after various leaching durations. Consequently, a novel method was proposed to calculate the activation energy based on boron-related structural units in the FTIR spectrum.

Compared to the ICP-OES method, the FTIR method accurately calculates the activation energy of boron at the onset of leaching and its evolution over the leaching duration. The FTIR method revealed the relationship between boron-related structural units and the activation energy. As the leaching reaction proceeds, the [BO_3] structure within the glass network gradually disappears, with the remaining space being occupied by molecular water. This increase in molecular water diminishes the [BO_3] intensity as observed in the infrared spectrum, consequently lowering the activation energy calculated via the FTIR method. The activation energy calculated using the FTIR method better reflects this change process.

CRediT authorship contribution statement

Kai Bai: Writing – review & editing, Writing – original draft, Investigation, Formal analysis, Data curation, Conceptualization. **Xiaofen Chen:** Resources. **Yuhe Pan:** Writing – review & editing, Formal analysis. **Zhaoxuan Jin:** Writing – review & editing. **Buyun Zhang:** Writing – review & editing, Validation. **Yuchuan Wang:** Data curation. **Peng Lv:** Writing – review & editing, Funding acquisition. **Tieshan Wang:** Funding acquisition. **Haibo Peng:** Writing – review & editing, Supervision, Funding acquisition.

Declaration of competing interest

The authors declare that they have no known competing financial interests or personal relationships that could have appeared to influence the work reported in this paper.

Data availability

Data will be made available on request.

Acknowledgments

This work was supported by the National Natural Science Foundation of China (Grant Nos. 12175092, U1867207), the Natural Science Foundation of Gansu Province (Grant Nos. 23JRRA1042, 23JRRA1145), and Haibo Peng was supported by INWARD coordinated research project [Ion Beam Irradiation for High-Level Nuclear Waste Form Development, F11022] from IAEA.

Supplementary materials

Supplementary material associated with this article can be found, in the online version, at doi:10.1016/j.jnoncrysol.2024.123244.

References

[1] S. Gin, P. Jollivet, M. Tribet, et al., Radionuclides containment in nuclear glasses: an overview, Radiochim. Acta 105 (11) (2017) 927–959.
[2] J. Sheng, S. Luo, B Tang, The leaching behavior of borate waste glass SL-1, Waste Manag. 19 (1999) 7.
[3] H. Jabraoui, T. Charpentier, S. Gin, et al., Atomic insights into the events governing the borosilicate glass–water interface, J. Phys. Chem. C 125 (14) (2021) 7919–7931.
[4] S. Gin, A. Abdelouas, L.J. Criscenti, et al., An international initiative on long-term behavior of high-level nuclear waste glass, Mater. Today 16 (6) (2013) 243–248.
[5] S. Luo, J. Sheng, B Tang, A comparison of HLW-glass and PWR-borate waste glass, JNuM 298 (2001) 4.
[6] V.I. Malkovsky, S.V. Yudintsev, M.I. Ojovan, et al., The influence of radiation on confinement properties of nuclear waste glasses, Sci. Technol. Nucl. Install. (2020) 2020.
[7] P. Frugier, T. Chave, S. Gin, et al., Application of the GRAAL model to leaching experiments with SON68 nuclear glass in initially pure water, J. Nucl. Mater. 392 (3) (2009) 552–567.
[8] S. Gin, J.M. Delaye, F. Angeli, et al., Aqueous alteration of silicate glass: state of knowledge and perspectives, NPJ Mater. Degrad. 5 (1) (2021).
[9] G.S. Frankel, J.D. Vienna, J. Lian, et al., A comparative review of the aqueous corrosion of glasses, crystalline ceramics, and metals, NPJ Mater. Degrad. 2 (1) (2018).
[10] M. Tribet, A.H. Mir, C. Gillet, et al., New insights about the importance of the alteration layer/glass interface, J. Phys. Chem. C 124 (18) (2020) 10032–10044.
[11] G.S. Frankel, J.D. Vienna, J. Lian, et al., Recent advances in corrosion science applicable to disposal of high-level nuclear waste, Chem. Rev. 121 (20) (2021) 12327–12383.
[12] J. Sheng, S Luo, 90U HLW-glass leaching mechanism in underground water original, JNuM 297 (1) (2001) 57–61.
[13] C. Cailleteau, F. Angeli, F. Devreux, et al., Insight into silicate-glass corrosion mechanisms, Nat. Mater. 7 (12) (2008) 978–983.
[14] R Conradt, Chemical durability of oxide glasses in aqueous solutions: a review, J. Am. Ceram. Soc. 91 (3) (2008) 728–735.
[15] S. Gin, C. Jegou, L. Sessegolo, et al., Effects of irradiation on the mechanisms controlling the residual rate of an alumino-borosilicate glass, NPJ Mater. Degrad. 6 (1) (2022) 1–14.
[16] J. Du, X. Lu, S. Gin, et al., Predicting the dissolution rate of borosilicate glasses using QSPR analysis based on molecular dynamics simulations, J. Am. Ceram. Soc. 104 (9) (2021) 4445–4458.
[17] L. Deng, K. Miyatani, M. Suehara, et al., Ion-exchange mechanisms and interfacial reaction kinetics during aqueous corrosion of sodium silicate glasses, NPJ Mater. Degrad. 5 (1) (2021) 1–13.
[18] R. Hellmann, S. Cotte, E. Cadel, et al., Nanometre-scale evidence for interfacial dissolution-reprecipitation control of silicate glass corrosion, Nat. Mater. 14 (3) (2015) 307–311.
[19] C. Lenting, O. Plümper, M. Kilburn, et al., Towards a unifying mechanistic model for silicate glass corrosion, NPJ Mater. Degrad. 2 (1) (2018).
[20] T. Geisler, T. Nagel, M.R. Kilburn, et al., The mechanism of borosilicate glass corrosion revisited, Geochim. Cosmochim. Acta 158 (2015) 112–129.
[21] P. Jollivet, P. Frugier, G. Parisot, et al., Effect of clayey groundwater on the dissolution rate of the simulated nuclear waste glass SON68, J. Nucl. Mater. 420 (1–3) (2012) 508–518.
[22] J. Neeway, A. Abdelouas, B. Grambow, et al., Vapor hydration of SON68 glass from 90 °C to 200 °C: a kinetic study and corrosion products investigation, J. Non Cryst. Solids 358 (21) (2012) 2894–2905.
[23] Y. Inagaki, T. Kikunaga, K. Idemitsu, et al., Initial dissolution rate of the international simple glass as a function of pH and temperature measured using microchannel flow-through test method, Int. J. Appl. Glass. Sci. 4 (4) (2013) 317–327.
[24] S. Mougnaud, M. Tribet, J.P. Renault, et al., Heavy ion radiation ageing impact on long-term glass alteration behavior, J. Nucl. Mater. 510 (2018) 168–177.
[25] R. Bouakkaz, A. Abdelouas, MENDILI Y El, et al., SON68 glass alteration under Si-rich solutions at low temperature (35–90°C): kinetics, secondary phases and isotopic exchange studies, RSC Adv. 6 (76) (2016) 72616–72633.
[26] W.L. Ebert, J.K. Bates, W.L Bourcier, The hydration of borosilicate waste glass in liquid and steam at 200°C, Waste Manag. 11 (1991) 205–221.
[27] S. Narayanasamy, P. Jollivet, L. Sessegolo, et al., Influence of temperature and relative humidity on vapor hydration of an AVM nuclear waste glass, J. Nucl. Mater. 543 (2021).
[28] C. Lenting, T Geisler, Corrosion of ternary borosilicate glass in acidic solution studied in operando by fluid-cell Raman spectroscopy, NPJ Mater. Degrad. 5 (1) (2021).

[29] D. Rébiscoul, F. Bruguier, V. Magnin, et al., Impact of soda-lime borosilicate glass composition on water penetration and water structure at the first time of alteration, J. Non Cryst. Solids 358 (22) (2012) 2951–2960.
[30] J.D. Vienna, J.J. Neeway, J.V. Ryan, et al., Impacts of glass composition, pH, and temperature on glass forward dissolution rate, NPJ Mater. Degrad. 2 (1) (2018).
[31] S. Narayanasamy, P. Jollivet, N. Godon, et al., Influence of composition of nuclear waste glasses on vapor phase hydration, J. Nucl. Mater. 525 (2019) 53–71.
[32] O.M. Farid, M.I. Ojovan, A. Massoud, et al., An assessment of initial leaching characteristics of alkali-borosilicate glasses for nuclear waste immobilization, Materials 12 (9) (2019) (Basel).
[33] C. Poinssot, S Gin, Long-term Behavior Science: the cornerstone approach for reliably assessing the long-term performance of nuclear waste, J. Nucl. Mater. 420 (1–3) (2012) 182–192.
[34] T.L. Goût, M.T. Harrison, I Farnan, Evaluating the temperature dependence of Magnox waste glass dissolution, J. Non Cryst. Solids 518 (2019) 75–84.
[35] O.M. Farid, M.I. Ojovan, R.O Abdel Rahman, Evolution of cations speciation during the initial leaching stage of alkali-borosilicate-glasses, MRS Adv. 5 (3–4) (2020) 185–193.
[36] M.I. Ojovan, A. Pankov, W.E Lee, The ion exchange phase in corrosion of nuclear waste glasses, JNuM 358 (1) (2006) 57–68.
[37] G. Leturcq, G. Berger, T. Advocat, et al., Initial and long-term dissolution rates of aluminosilicate glasses enriched with Ti, Zr and Nd, ChGeo 160 (1–2) (1999) 39–62.
[38] Helgeson H C, Murphy W M, Aagaard P. Thermodynamic and kinetic constraints on reaction rates among minerals and aqueous solutions. II. Rate constants, effective surface area, and the hydrolysis of feldspar [J]. Geochimica et Cosmochimica Acta, 48: 2405-32.
[39] C. Jegou, S. Narayanasamy, F Angeli, Short communication on the Influence of the temperature between 30 and 70°C on the hydration of SON68 nuclear waste glass in a vapour phase, J. Nucl. Mater. 545 (2021).
[40] P. Zapol, H. He, K.D. Kwon, et al., First-principles study of hydrolysis reaction barriers in a sodium borosilicate glass, Int. J. Appl. Glass. Sci. 4 (4) (2013) 395–407.
[41] K. Qin, B. Zhang, Z. Jin, et al., Influence of radiation on borosilicate glass leaching behaviors, NPJ Mater. Degrad. 8 (1) (2024).
[42] S. Zhu, Z. Jin, B. Zhang, et al., Electron irradiation-induced elements depletion and macroscopic changes in ternary borosilicate glasses: mechanism and composition dependence, Appl. Surf. Sci. 654 (2024).
[43] C.W. Kim, J.K. Park, T.W Hwang, Analysis of leaching behavior of simulated LILW glasses by using the MCC-1 test method, J. Nucl. Sci. Technol. 48 (7) (2011) 1108–1114.
[44] S.C Slate, Standardized waste form test methods, Mater. Res. Soc. 44 (1985).
[45] X.Y. Zhang, F. Yang, S.K. Zhu, et al., Influence of ion radiation on leaching behavior of borosilicate glass, J. Non Cryst. Solids 602 (2023) 122091.
[46] P. Jollivet, S. Gin, S Schumacher, Forward dissolution rate of silicate glasses of nuclear interest in clay-equilibrated groundwater, Chem. Geol. 330-331 (2012) 207–217.
[47] S. Gin, X. Guo, J.M. Delaye, et al., Insights into the mechanisms controlling the residual corrosion rate of borosilicate glasses, NPJ Mater. Degrad. 4 (1) (2020) 41.
[48] E.L. Abo-Naf S M, F.H. Batal, M.A. Azooz, Characterization of some glasses in the system SiO2, Na2O· RO by infrared spectroscopy, MCP 77 (3) (2003) 846–852.
[49] E.I. Kamitsos, A.P. Patsis, G.D Chryssikos, Infrared reflectance investigation of alkali diborate glasses, J. Non Cryst. Solids 152 (1993) 246–256.
[50] R.D. Husung, R.H Doremus, The infrared transmission spectra of four silicate glasses before and after exposure to water, J. Mater. Res. (1990).
[51] P.K. Jha, O.P. Pandey, K Singh, FTIR spectral analysis and mechanical properties of sodium phosphate glass–ceramics, JMoSt 1083 (2015) 278–285.
[52] M. Vallet-Regí, E. Romero, C. Ragel, et al., XRD, SEM-EDS, and FTIR studies of in vitro growth of an apatite-like layer on sol-gel glasses, J. Biomed. Mater. Res. Off. J. Soc. Biomater. Jpn. Soc. Biomater. Aust. Soc. Biomater. 44 (4) (1999) 416–421.
[53] A. Aronne, S. Esposito, P Pernice, FTIR and DTA study of structural transformations and crystallisation in BaO–B2O3–TiO2 glasses, Phys. Chem. Glass. 40 (2) (1999) 63–68.
[54] M. Lobanova, A. Ledieu, P. Barboux, et al., Effect of ZrO2 on the glass durability, Mater. Res. Soc. 713 (2002) JJ15.1.1–JJ15.1.9.
[55] X. Lu, L. Deng, S. Kerisit, et al., Structural role of ZrO2 and its impact on properties of boroaluminosilicate nuclear waste glasses, NPJ Mater. Degrad. 2 (1) (2018).
[56] I. Hussain, E.K. Barimah, Y. Iqbal, et al., Mechanical and optical properties of ZrO2 doped silicate glass ceramics, Silicon 13 (3) (2020) 877–883.
[57] A.J. Connelly, N.C. Hyatt, K.P. Travis, et al., The structural role of Zr within alkali borosilicate glasses for nuclear waste immobilisation, J. Non Cryst. Solids 357 (7) (2011) 1647–1656.
[58] S. Gin, L. Neill, M. Fournier, et al., The controversial role of inter-diffusion in glass alteration, Chem. Geol. 440 (2016) 115–123.
[59] S. Gin, C. Guittonneau, N. Godon, et al., Nuclear glass durability: new insight into alteration layer properties, J. Phys. Chem. C 115 (38) (2011) 18696–18706.
[60] P. Frugier, S. Gin, Y. Minet, et al., SON68 nuclear glass dissolution kinetics: current state of knowledge and basis of the new GRAAL model, J. Nucl. Mater. 380 (1–3) (2008) 8–21.
[61] C. Guy, J Schott, Multisite surface reaction versus transport control during the hydrolysis of a complex oxide, Chem. Geol. 78 (1989) 181–204.
[62] D. Ngo, H. Liu, N. Sheth, et al., Spectroscopic ellipsometry study of thickness and porosity of the alteration layer formed on international simple glass surface in aqueous corrosion conditions, NPJ Mater. Degrad. 2 (1) (2018).
[63] H. Arena, R. Podor, H.P. Brau, et al., Characterization of the boron profile and coordination in altered glass layers by EEL spectroscopy, Micron 141 (2021) 102983.